A rolling-diaphragm hydrostatic transmission for remote MR-guided needle insertion

Natalie Burkhard[1], Samuel Frishman[1], Alexander Gruebele[1], J. Peter Whitney[2]
Roger Goldman[3], Bruce Daniel[3], Mark Cutkosky[1]

Abstract— Magnetic resonance imaging (MRI) offers many benefits, including unsurpassed soft-tissue characterization and the ability to combine detection and biopsy into a single procedure. However, limited patient access in the narrow scanner bore requires tedious iterative positioning or use of robotic assistants that isolate the physician from the patient. As an alternative, we present a teleoperation technology for percutaneous procedures to meet the needs of interventional radiologists and overcome challenges imposed by the MR environment. The technology is demonstrated for a 1-DOF needle insertion procedure. The technology uses rolling diaphragms, a clutch, and a cable-capstan drive to propel the needle while relaying forces and motions to the operator. The system demonstrates excellent position tracking ($< 0.7°$ error in the unloaded case) and reliably transmits changes in force. During needle teleoperation, users were able to detect light membrane punctures and differentiate spring stiffnesses nearly as accurately as by hand manipulation.

I. INTRODUCTION

A. Motivation and Application

Use of diagnostic MRI in the USA quadrupled from 1996-2010 with 30.2M procedures in 2010 alone [1]. Increasingly, physicians want to use MRI not only for diagnosis but also for guided procedures [2]. This combination offers revolutionary capabilities but also presents challenges, including limited patient access. Patients are repeatedly extracted from the bore to let physicians iteratively position tools between scans in an approach that does not take advantage of real-time imaging and is susceptible to anatomy shifts [2]. Robotic solutions can improve access and tool positioning accuracy, but MR-compatibility requirements constrain their design and limit transparency [3], preventing the physician from feeling tool/tissue interaction forces. These devices isolate patients from physicians, forcing them to rely on visual cues. The benefits of haptic feedback – including improved accuracy, faster task times, and enhanced learning – have been demonstrated for other teleoperated tasks. Physicians want haptic feedback and find, after years of practice, that they rely on feel as much as vision for some procedures [4], such as membrane puncture or identification of dense tissue.

To address this need, we present a novel bilateral teleoperator that naturally extends physicians' hands to enable remote tool positioning under MR, application of appropriate forces, and identification of tissue properties. The teleoperator relies on a hydrostatic transmission [5] with rolling diaphragms, which eliminate sliding seals, pumps, and valves for a combination of high stiffness and low friction, inertia and backlash [6]. Its haptic capabilities arise from its high stiffness and transparency, or ability to reflect forces and motions between the master (input) and slave (remote output, where the tool is held). Unlike many existing MR-compatible robotic teleoperators, it is completely passive and backdrivable, which requires no virtual environment, guarantees stability, and improves safety by keeping the interventionalist in the loop.

A compelling first application is MR-guided transperineal needle placement for prostate biopsy. One in six American men will be diagnosed with prostate cancer during his lifespan [7], and prostate biopsy is a prerequisite for determining optimal treatment [8]. Transperineal biopsy is a safe, sterile path toward prostate targets that can immediately follow tumor detection during a single outpatient procedure. Biopsy needles are conventionally placed using template-based systems, needle holders, or freehand [8]. The patient is moved into and out of the scanner to iteratively manipulate the needle through ~7 cm of tissue from between the patient's legs to a precise target in the prostate near the center of the long, narrow MRI bore. These "point and shoot" methods involve ample trial and error. The presented device is an important part of a solution for simultaneous imaging and needle insertion with haptic feedback.

B. Related prior work

MR-compatible surgical aids face major technical challenges due to the strong magnetic fields and gradients, electromagnetic interference, and confined workspace in the scanner [9]. These realities severely constrain the design choices – precluding many conventional actuators and sensors – to ensure safety and maintain accuracy (e.g., to minimize artifacts). Suitable devices have been developed for percutaneous interventions, as reviewed in [10].

Several groups address the specific problems of MR-guided prostate biopsy, and many are reviewed in [8]. As noted, various non-robotic approaches exist but suffer from time-consuming, iterative needle guide positioning [11] and do not permit simultaneous imaging and needle insertion. Some robotic approaches are designed to work with open MR scanners [12] because they offer improved patient accessibility, but these scanners do not provide high image

[1]Department of Mechanical Engineering, Stanford University, Stanford, CA 94305 `ntb@, samuel9@, agruebe2@, cutkosky@stanford.edu`

[2]Department of Mechanical and Industrial Engineering, Northeastern University, Boston, MA 02115 `j.whitney@neu.edu`

[3]Department of Radiology, Stanford University, Stanford, CA 94305 `goldmanr@, bdaniel@stanford.edu`

quality and often rely on registration to pre-operative images, further reducing accuracy [8]. We are designing for closed-bore scanners. Others are intended for a transgluteal [13] or transrectal [11], [14], [15] approach; we prefer transperineal for its safety, sterility, and relative ease in avoiding delicate structures or pubic arch interference. It also enables access to regions of the prostate that transrectal approaches cannot reach [16]. Other designs are active, relying on pneumatic [17]–[19], hydraulic, ultrasonic [12], [20], piezoelectric [21], or dielectric elastomer [22] actuators for needle positioning and/or insertion. An example of a passive robot specifically designed for MR-guided transperineal prostate biopsy in a closed scanner is the parallel-chain master/slave linkage described in [4] and [23].

Here we focus on accurate motion transmission and haptic sensitivity and adopt a rolling-diaphragm hydrostatic system for its flexibility of design and application. Although demonstrated here for a linear 1-DOF task, the transmission is easily converted to rotary motion or expanded to multi-DOF motions. The transmission is adapted from human-interaction robots [6], [24] with accurate, passive feedback of forces and motions between master and slave [5]. The working fluid is water, and all components of the transmission can be made from non-magnetic materials.

II. FORCE AND MOTION REQUIREMENTS

The device must provide sufficient needle displacement (~7 cm) and withstand the range of forces experienced during transperineal biopsy while maintaining sufficient position and force tracking accuracy between input and output to detect events of interest. The "gold standard" against which to compare a teleoperated system is direct manipulation of the needle with the fingers. However, any guide system or apparatus will affect the forces experienced. Note also that physicians often do not insert the entire needle in a single stroke: they grasp the needle part way along its length, make an initial insertion motion, and then re-grasp to complete the insertion.

Clinical studies show that needle placement errors for percutaneous tasks may be due to imaging limitations (± 5 mm), human error, target movement due to tissue deformation or gland motion/swelling (± 6.5 mm), and needle deflection [25]. Other prostate biopsy devices that claim the ability to puncture most clinically relevant tumors report errors of $\sim 2 - 3$ mm with maximum errors of $\sim 3 - 6$ mm [26].

In vivo measurements for manual 18 gauge (1.27mm) needle insertion in human soft tissue have shown that maximum insertion force is ~ 5 N for the prostate capsule [27] (a perineal incision is made to ease needle access). Membrane punctures with 18 gauge needles result in 0.2-1.5 N changes in axial force [27]–[30]. However, human force perception also limits what is felt. Several studies have indicated that the just-noticeable-difference (JND) in force magnitude is 5-10% of the reference force [31]–[33]. Similarly, the JND for changes in stiffness during interactions with soft environments is 8-12% of the reference for a 75% detection rate [34]. However, all of these JND studies involved passive sensing
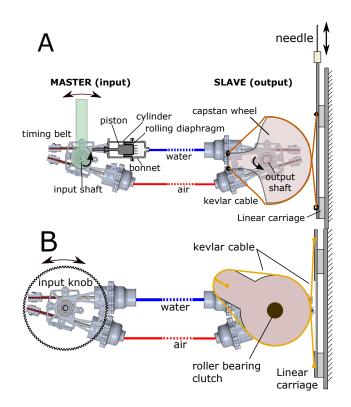

Fig. 1. (*A:*) Master and slave sides of the transmission use paired rolling diaphragm actuators. One line is water-filled for stiffness; the other contains pressurized air. The slave side uses a capstan/cable drive to propel the needle on a linear track. (*B:*) Modified version uses knob for enhanced tactile sensitivity and smaller capstan wheel. A roller bearing clutch allows 2+ input rotations (~45° each) over full travel of needle.

tasks in highly controlled environments, and participants were not wearing gloves; JND values are likely higher for doctors performing transperineal biopsy. Our design specifications are thus as follows:

1) Force tracking errors of $< 15\%$ of the reference force over 0-6 N.
2) Position tracking errors < 2 mm on average and < 5 mm at maximum over 0-10 cm.
3) Users can detect membrane puncture during needle insertion into phantom tissue with 90% accuracy.
4) Users can detect relative changes in stiffness of 20%.

III. METHODS

A. Design

A hybrid air/water version of the rotary transmission presented in [6], [24] was selected to reflect forces and motions while minimizing use of metal tubing. In this variant, a single water-filled line maintains stiffness and a second, thinner and more flexible line with pressurized air maintains a positive pressure under all conditions (Fig. 1). Opposed rolling diaphragm actuators are located at each end and connected via a timing belt to a rotary joint. When properly degassed and tensioned, the system has tracking errors of $< 0.5^o$ under light loads. Although the current prototype has a few ferrous components (Fig. 2), it is simple to substitute them with aluminum, brass, ceramics, and/or polymers for tests under MR.
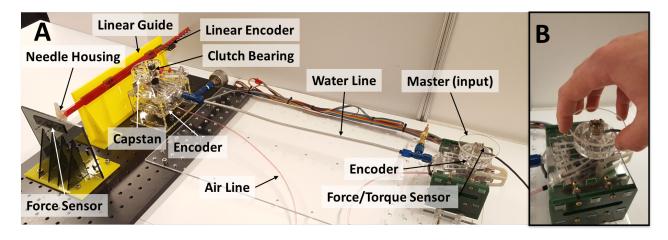
Fig. 2. *A:* The 1-DoF transmission system with associated sensors for characterizing force and position transparency. Optical encoders track input and output rotation as well as linear displacement of the needle. Force sensors measure the input torque and force experienced at the needle tip. *B:* Input knob for heightened tactile sensitivity.

At the needle side, we convert rotary to linear motion using a capstan drive, as commonly used in haptic devices for its combination of low friction, smoothness and high stiffness. The initial version of the device, shown in Fig. 1A, has a lever at the input and uses a single stroke to drive the needle. The rolling diaphragms limit the actuators to 24 mm stroke, or 135° of rotation at the rotary joints. The initial version has a ⌀65 mm capstan wheel, giving 51mm of needle travel for 45° rotation.

After conducting user tests (see Sections IV-B and IV-C) and obtaining user feedback, a second version of the apparatus was created. It was motivated by the observation that physicians often drive the biopsy needle with multiple motions, regrasping between strokes. It has a textured circular knob (⌀63.5 mm) at the input and a smaller sector pulley (⌀44.5 mm) at the output, giving 45° per 35 mm of needle travel. The textured knob, inspired by knurled tools used for precise handwork, enhances tactile sensitivity. This, in combination with a more favorable transmission ratio, makes it easier to detect small changes in force.

The needle moves a total of 10 cm along a pair of rails using low-friction linear bearings. To achieve sufficient linear displacement from the rotational motion, a needle-roller bearing clutch (McMaster #6392K42) connects the output shaft to the sector pulley. This arrangement allows multiple rotations of the input to drive the needle the full distance. The effect is roughly analogous to the act of lifting up a computer mouse to recenter it on a mouse pad. As noted in previous work on haptics, users tolerate this "clutching" behavior well in exchange for greater resolution [35]. The incremental motion results in smaller piston displacements and enables the system to utilize the optimal middle sections of the rolling diaphragms. For needle retraction, the design requires disengagement of the bearing clutch from the output shaft. This is currently achieved with a set screw. The design can be modified to include a second clutch that enables a user to smoothly toggle between insertion and retraction.

B. Transparency Performance

For system characterization of the second version of the system, we mounted a force/torque sensor (ATI Nano, ∼3.1 mN resolution) between the input shaft and textured knob to measure input forces. We attached a second load cell (Honeywell FSG015WNPB, ∼9.8 mN resolution) to a vertical plate, against which the needle is driven in order to record axial needle forces. Rotary optical encoders (5000 CPR with quadrature) tracked rotations at input and output shafts and a linear encoder (1000 counts/inch) tracked linear carriage motion. Figure 2 shows the experimental setup. Data were recorded with a custom C++ program and an Arduino Due, filtered using a third order zero-phase filter, and analyzed in MatLab. We manipulated the system under no-load conditions and with the needle guide pressed against a variety of springs.

C. User Tests

We conducted tests using the first version of the system (Fig. 1A) to measure users' ability to detect membrane puncture events and to distinguish between different stiffness levels using the teleoperator versus manipulating the needle directly. During teleoperation, subjects were instructed to
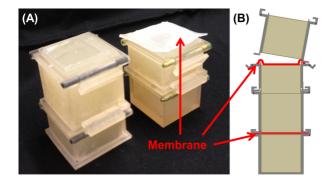

Fig. 3. Reconfigurable membrane and tissue phantom (A) photo and (B) assembly diagram as shown in [23].

grasp a lightweight handle with two fingers and advised to move slowly and steadily. Puncture tests were conducted in agar phantom blocks separated by ∼0.2 mm silicone membranes (Dragon Skin FX-Pro, Smooth On Inc, Easton, PA) with embedded tissue (34155, Kimwipes, Kimberly-Clark, Irving, TX) at random depths in the agar (Fig. 3) [4]. Subjects were instructed to stop needle insertion when they encountered a membrane; success occurred if they stopped within 5mm. Seven subjects (3 women, 4 men, ages 25-30) were tested. Stiffness tests required subjects to rank the relative stiffness of 5 springs ($k = 0.33, 0.57, 0.82, 1.54$, and 2.86 N/mm) mounted to a hard surface. Subjects were permitted to feel springs multiple times until sure of the springs' stiffness order. The 5 springs were first presented to subjects in randomized order and then again on subjects' demand. 8 subjects (5 women, 3 men, ages 25-30) were tested.

IV. RESULTS

A. Transparency Performance

No-load position tracking errors with the second version of the apparatus (Fig. 1B) averaged 0.30mm with a 0.55mm maximum over 8cm. This is well below the design specification. The angles of the master and slave are denoted by θ_m and θ_s, respectively. The corresponding needle motion (i.e., needle translation divided by sector pulley radius) is labeled X_n/R. To account for the "clutching" motion, the rotation is divided into three regions (see Fig. 4). Region A is defined as the initial forward stroke of the master in which the master drives the slave and needle. Region B is defined as the reverse stroke of the master, during which the slave and needle remain stationary. Region C is the second forward stroke of the master. The reverse angle of the master in Region B is labeled θ_c and represents the offset angle between the input and output. This offset angle is added to the difference between the Master-Needle and Master-Slave pairs when calculating the displacement error in Region C.

Figure 5 shows position and force tracking results when the needle is pressed against soft (1.19 N/mm) or stiff (4.94 N/mm) springs. The position error averaged 0.44 mm for the soft spring and 0.68 mm for the stiff spring. The magnitude of the force difference averaged 0.86 N for the soft spring and 0.66 N for the stiff spring over the 0-6 N range. This is below the 15% force transmission design specification for both cases (14% and 11% for the two cases). Note that these force differences include the force required at the input to move the apparatus in air, which can be on the order of 1N, (per Fig. 4) for moderate motions.

B. Membrane Puncture Detection

User tests did not reveal any issues with mapping rotary input to linear needle motion. Membrane punctures had an average of 77% success (standard deviation was 9%, range = 63-88%). Puncture forces were realistically sized on the lighter end of membranes one would encounter in transperineal prostate biopsy, ranging from 0.31-0.66 N
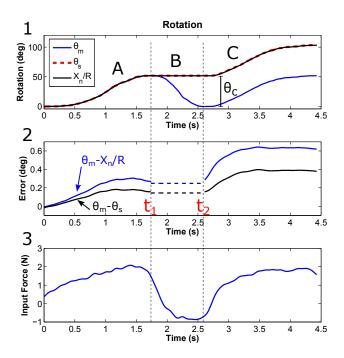

Fig. 4. *(1)*: No-load position tracking. θ_m is input rotation; θ_s is output rotation. Region A is the first forward stroke; region B is a reverse stroke, and region C is the second stroke. Full range of actuator not demonstrated here. *(2)*: Errors in region C are accumulated from the first and second strokes. The largest error, $\theta_m - X_n/R$ from input to needle travel, remains $< 0.7°$. *(3)*: Input force is nonzero due to system inertia, hysteresis, and friction, and increases with input displacement.

(average = 0.48N, standard deviation 0.10). All users had 100% accuracy with the handheld needle.

C. Spring Stiffness Ranking

No subject test took longer than 10 minutes, including instructions; most took < 5 minutes. Each subject presented their spring stiffness ranking; these results were used to determine how often each pair of springs were confused. Users had 100% accuracy in distinguishing all pairs of spring combinations except two: 88% accuracy in distinguishing 2.86 N/mm and 1.54 N/mm (46% relative stiffness difference), and 63% accuracy for 0.82 N/mm and 0.57 N/mm (31% relative stiffness difference).

V. DISCUSSION

As anticipated, the hydrostatic transmission results in a system that reproduces input motions at the master to corresponding motions at the slave. In comparison to other approaches (e.g. linkages or cables) it is relatively stiff, provided that air is carefully removed from the water transmission line. A more thorough approach for degassing the line is a topic of ongoing work. It is noted that these fluid lines were relatively short (30 cm); slightly diminished performance is expected with increased distance between master and slave sides. Fluidic losses are expected to remain minimal for the given pipe diameters ($\frac{1}{4}$ inch water and $\frac{1}{8}$ inch air) and relatively small flow rates.

An ideal transmission would also be mass-less and devoid of hysteretic or frictional forces. However, the apparatus used for these tests has some inertia and some losses, primarily
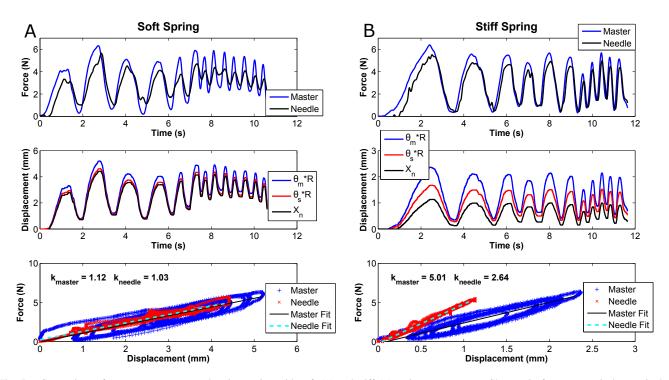
Fig. 5. Comparison of system transparency when interacting with soft (*A*) and stiff (*B*) springs. *Upper row*: Changes in force are tracked; magnitudes are expressed with a small lag and higher relative accuracy in the stiff case. *Middle row*: Displacement errors are approximately equal in the soft and stiff cases. *Bottom row*: Stiffness as experienced by the input (master) and output (needle). For the soft spring, input stiffness matches endpoint stiffness ($1.19\,\text{N/mm}$); for the stiff spring ($4.94\,\text{N/mm}$), elasticity in the apparatus contributes noticeably to the apparent stiffness at the master.

in the diaphragms themselves as they roll. Viscous damping (Poiseuille flow) losses are minor for the given tubing diameter and velocity. In addition to air bubbles, compliance also results from the plastic structural components used to support the needle and its linear carriage. As a result of these effects, forces of approximately $1.3\,\text{N}$ are required to move the apparatus back and forth, even in the absence of any needle forces. However, as can be seen in Fig. 5, these forces are relatively independent of needle force and needle velocity. Therefore, when the needle encounters a change in stiffness, the difference in needle force is tracked proportionally at the input, particularly if the velocity remains relatively constant.

Operating the device in the intermediate stroke range of the rolling diaphragms also improves the force transparency because hysteretic losses and a elastic restoring force associated with the diaphragms are most apparent near the ends of travel. This finding motivated the clutching mechanism used for the second version of the device.

Although users were unable to detect membrane punctures with 90% accuracy, we believe that their performance (77% accuracy) was excellent given a few key points. Although our membranes had realistic puncture forces (0.3-$0.66\,\text{N}$), they were on the lighter side of in-vivo values (0.2-$1.5\,\text{N}$). Furthermore, user tests were conducted using the first version of the device, which did not have the knurled input handle for tactile sensibility or a clutching mechanism, and thus allowed users to operate near the ends of the rolling diaphragm. Similar factors may have affected the results of the user test for distinguishing spring stiffnesses: users only had trouble with 2 of 10 spring pairs ($\binom{5}{2} = 10$ pairs), both of which were difficult to distinguish by hand. Furthermore, all

subjects were non-experts; it is possible that interventional radiologists will be more skilled at these tasks.

VI. CONCLUSIONS AND FUTURE WORK

Results with the 1-DoF hydrostatic teleoperation prototype are encouraging: it can transmit forces and motions repeatably and transparently. Force accuracy and stiffness discrimination are sufficient for clinical relevance. Performance is better at low speeds due to inertial loads. The simplicity and guaranteed safety of this system will facilitate its use. The presented work is a step toward reductions in time and cost for MR-guided interventions by enabling simultaneous imaging and tool manipulation. It will expand what interventions are feasible and the level of accuracy to which they may be performed.

Immediate improvements are to modify the apparatus to reduce inertia and hysteretic losses, and to increase the stiffness of the apparatus. The next step is to build a multi-DoF version suitable for needle manipulation, and to implement device registration to MR images.

REFERENCES

[1] R. Smith-Bindman, D. L. Miglioretti, E. Johnson, C. Lee, H. S. Feigelson, M. Flynn, R. T. Greenlee, R. L. Kruger, M. C. Hornbrook, D. Roblin, L. I. Solberg, N. Vanneman, D. L. Miglioretti, E. Johnson, C. Lee, H. S. Feigelson, M. Flynn, R. T. Greenlee, R. L. Kruger, M. C. Hornbrook, D. Roblin, L. I. Solberg, N. Vanneman, S. Weinmann, and A. E. Williams, "Use of Diagnostic Imaging Studies and Associated Radiation Exposure for Patients Enrolled in Large Integrated Health Care Systems, 1996-2010," *J. Am. Med. Assoc.*, vol. 307, no. 22, pp. 2400–2409, 2012.

[2] N. V. Tsekos, A. Khanicheh, E. Christoforou, and C. Mavroidis, "Magnetic resonance-compatible robotic and mechatronics systems for image-guided interventions and rehabilitation: a review study." *Annu. Rev. Biomed. Eng.*, vol. 9, no. 1, pp. 351–387, 2007.

[3] K. Chinzei, R. Kikinis, and F. Jolesz, "MR compatibility of mechatronic devices: Design criteria," in *Med. Image Comput. Comput. Assist. Interv.*, 1999, pp. 1020–1030.

[4] S. Elayaperumal, J. H. Bae, B. L. Daniel, and M. R. Cutkosky, "Detection of membrane puncture with haptic feedback using a tip-force sensing needle," in *Int. Conf. Intell. Robot. Syst.*, 2014, pp. 3975–3981.

[5] G. Ganesh, R. Gassert, E. Burdet, and H. Bleuler, "Dynamics and Control of an MRI Compatible Master-Slave System with Hydrostatic Transmission," in *Int. Conf. Robot. Autom.*, vol. 2, 2004, pp. 1288–1294.

[6] J. P. Whitney, M. F. Glisson, E. L. Brockmeyer, and J. K. Hodgins, "A Low-Friction Passive Fluid Transmission and Fluid-Tendon Soft Actuator," in *Int. Conf. Intell. Robot. Syst.*, 2014, pp. 2801–2808.

[7] J. C. Blasko, T. Mate, J. E. Sylvester, P. D. Grimm, and W. Cavanagh, "Brachytherapy for carcinoma of the prostate: techniques, patient selection, and clinical outcomes," in *Semin. Radiat. Oncol.*, vol. 12, no. 1. Elsevier, 2002, pp. 81–94.

[8] K. M. Pondman, J. J. Fütterer, B. ten Haken, L. J. Schultze Kool, J. A. Witjes, T. Hambrock, K. J. Macura, and J. O. Barentsz, "MR-Guided Biopsy of the Prostate: An Overview of Techniques and a Systematic Review," *Eur. Urol.*, vol. 54, no. 3, pp. 517–527, 2008.

[9] R. Gassert, E. Burdet, and K. Chinzei, "Opportunities and challenges in MR-compatible robotics," *IEEE Eng. Med. Biol. Mag.*, vol. 27, no. 3, pp. 15–22, 2008.

[10] M. M. Arnolli, N. C. Hanumara, M. Franken, D. M. Brouwer, and I. A. M. J. Broeders, "An overview of systems for CT- and MRI-guided percutaneous needle placement in the thorax and abdomen," *Int. J. Med. Robot. Comput. Assist. Surg.*, vol. 11, pp. 458–475, 2015.

[11] D. Beyersdorff, A. Winkel, B. Hamm, S. Lenk, S. A. Loening, and M. Taupitz, "MR Imaging-guided Prostate Biopsy with a Closed MR Unit at 1.5 T: Initial Results," *Radiology*, vol. 234, no. 2, pp. 576–581, 2005.

[12] S. P. DiMaio, S. Pieper, K. Chinzei, N. Hata, S. J. Haker, D. F. Kacher, G. Fichtinger, C. M. Tempany, and R. Kikinis, "Robot-assisted needle placement in open MRI: system architecture, integration and validation." *Comput. Aided Surg.*, vol. 12, no. 1, pp. 15–24, 2007.

[13] S. Zangos, C. Herzog, K. Eichler, R. Hammerstingl, A. Lukoschek, S. Guthmann, B. Gutmann, U. J. Schoepf, P. Costello, and T. J. Vogl, "MR-compatible assistance system for punction in a high-field system: Device and feasibility of transgluteal biopsies of the prostate gland," *Eur. Radiol.*, vol. 17, no. 4, pp. 1118–1124, 2007.

[14] K. Engelhard, H. P. Hollenbach, B. Kiefer, A. Winkel, K. Goeb, and D. Engehausen, "Prostate biopsy in the supine position in a standard 1.5-T scanner under real time MR-imaging control using a MR-compatible endorectal biopsy device," *Eur. Radiol.*, vol. 16, no. 6, pp. 1237–1243, 2006.

[15] G. Fichtinger, A. Krieger, R. C. Susil, A. Tanacs, L. Whitcomb, and E. Atalar, "Transrectal Prostate Biopsy Inside Closed MRI Scanner with Remote Actuation, under Real-Time Image Guidance," in *Med. Image Comput. Comput. Assist. Interv.*, 2002, pp. 91–98.

[16] P. Acher and M. Dooldeniya, "Prostate biopsy: Will transperineal replace transrectal?" *BJU Int.*, vol. 112, no. 5, pp. 533–534, 2013.

[17] G. S. Fischer, I. Iordachita, C. Csoma, J. Tokuda, S. P. DiMaio, C. M. Tempany, N. Hata, and G. Fichtinger, "MRI-compatible pneumatic robot for transperineal prostate needle placement," *IEEE/ASME Trans. Mechatronics*, vol. 13, no. 3, pp. 295–305, 2008.

[18] S.-E. E. Song, N. B. Cho, G. Fischer, N. Hata, C. Tempany, G. Fichtinger, and I. Iordachita, "Development of a Pneumatic Robot for MRI-guided Transperineal Prostate Biopsy and Brachytherapy: New Approaches," in *Int. Conf. Robot. Autom.*, 2010, pp. 2580–2585.

[19] M. R. van den Bosch, M. R. Moman, M. van Vulpen, J. J. Battermann, E. Duiveman, L. J. van Schelven, H. de Leeuw, J. J. W. Lagendijk, and M. a. Moerland, "MRI-guided robotic system for transperineal prostate interventions: proof of principle." *Phys. Med. Biol.*, vol. 55, no. 5, pp. N133–40, 2010.

[20] K. Masamune, E. Kobayashi, Y. Masutani, M. Suzuki, T. Dohi, H. Iseki, and K. Takakura, "Development of an MRI-compatible needle insertion manipulator for stereotactic neurosurgery." *J. Image Guid. Surg.*, vol. 1, no. 4, pp. 242–248, 1995.

[21] S. E. Song, J. Tokuda, K. Tuncali, A. Yamada, M. Torabi, and N. Hata, "Design evaluation of a double ring RCM mechanism for robotic needle guidance in MRI-guided liver interventions," in *Int. Conf. Intell. Robot. Syst.*, 2013, pp. 4078–4083.

[22] K. Tadakuma, L. M. DeVita, J. S. Plante, Y. Shaoze, and S. Dubowsky, "The experimental study of a precision parallel manipulator with binary actuation: With application to MRI cancer treatment," in *Int. Conf. Robot. Autom.*, 2008, pp. 2503–2508.

[23] S. Elayaperumal, M. R. Cutkosky, P. Renaud, and B. L. Daniel, "A Passive Parallel MasterSlave Mechanism for Magnetic Resonance Imaging-Guided Interventions," *J. Med. Device.*, vol. 9, no. 1, pp. 011 008–1, 2015.

[24] J. P. Whitney, T. Chen, J. Mars, and J. K. Hodgins, "A Hybrid Hydrostatic Transmission and Human-Safe Haptic Telepresence Robot," in *Int. Conf. Robot. Autom.*, 2016, pp. 690–695.

[25] N. Abolhassani, R. Patel, and M. Moallem, "Needle insertion into soft tissue: A survey," *Med. Eng. Phys.*, vol. 29, no. 4, pp. 413–431, 2007.

[26] M. G. Schouten, J. Ansems, W. K. J. Renema, D. Bosboom, T. W. J. Scheenen, and J. J. Fütterer, "The accuracy and safety aspects of a novel robotic needle guide manipulator to perform transrectal prostate biopsies." *Med. Phys.*, vol. 37, no. 9, pp. 4744–4750, 2010.

[27] T. Podder, D. Clark, J. Sherman, D. Fuller, E. Messing, D. Rubens, J. Strang, R. Brasacchio, L. Liao, W.-S. Ng, and Y. Yu, "Vivo motion and force measurement of surgical needle intervention during prostate brachytherapy." *Med. Phys.*, vol. 33, no. 2006, pp. 2915–2922, 2006.

[28] B. Maurin, L. Barbe, B. Bayle, P. Zanne, J. Gangloff, M. de Mathelin, A. Gangi, L. Soler, and A. Forgione, "In vivo study of forces during needle insertions," in *Proc. Sci. Work. Med. Robot. Navig. Vis.*, 2004, pp. 1–8.

[29] A. M. Okamura, C. Simone, and M. D. O'Leary, "Force modeling for needle insertion into soft tissue," *IEEE Trans. Biomed. Eng.*, vol. 51, no. 10, pp. 1707–1716, 2004.

[30] C. Simone and A. Okamura, "Modeling of needle insertion forces for robot-assisted percutaneous therapy," in *Int. Conf. Robot. Autom.*, 2002, pp. 2085–2091.

[31] L. A. Jones, "Matching forces: constant errors and differential thresholds," *Perception*, vol. 18, no. 5, pp. 681–687, 1989.

[32] X. D. Pang, H. Z. Tan, and N. I. Durlach, "Manual discrimination of force using active finger motion." *Percept. Psychophys.*, vol. 49, no. 6, pp. 531–540, 1991.

[33] H. Z. Tan, M. A. Srinivasan, B. Eberman, and B. Cheng, "Human factors for the design of force-reflecting haptic interfaces," *ASME J. Dyn. Syst.*, vol. 55, no. 1, pp. 353–359, 1994.

[34] G. De Gersem, H. V. Brussel, and F. Tendick, "Reliable and Enhanced Stiffness Perception in Soft-tissue Telemanipulation," *Int. J. Rob. Res.*, vol. 24, no. 10, pp. 805–822, 2005.

[35] F. Conti and O. Khatib, "Spanning large workspaces using small haptic devices," in *World Haptics Conf.*, 2005, pp. 183–188.